Eur. J. Biochem. **268,** 4885–4891 (2001) © FEBS 2001

All or none fibrillogenesis of a prion peptide

Wen-Quan Zou[1], Dun-Sheng Yang[1], Paul E. Fraser[1,2], Neil R. Cashman[1] and Avijit Chakrabartty[2]

[1]*Centre for Research in Neurodegenerative Diseases, and* [2]*Department of Medical Biophysics, University of Toronto, Ontario, Canada*

Amyloid proteins and peptides comprise a diverse group of molecules that vary both in size and amino-acid sequence, yet assemble into amyloid fibrils that have a common core structure. Kinetic studies of amyloid fibrillogenesis have revealed that certain amyloid proteins form oligomeric intermediates prior to fibril formation. We have investigated fibril formation with a peptide corresponding to residues 195–213 of the human prion protein. Through a combination of kinetic and equilibrium studies, we have found that the fibrillogenesis of this peptide proceeds as an all-or-none reaction where oligomeric intermediates are not stably populated. This variation in whether oligomeric intermediates are stably populated during fibril formation indicates that amyloid proteins assemble into a common fibrillar structure; however, they do so through different pathways.

Keywords: fibrillogenesis; prion peptide; fluorescence resonance energy transfer.

Amyloid diseases comprise a diverse group of conditions that are characterized by conformational conversion of soluble proteins into insoluble amyloid fibrils, which deposit in tissues such as the heart, liver, spleen, and brain [1]. While amyloid proteins differ from disease to disease, and differ vastly in size and sequence, the structure of all amyloid fibrils are strikingly similar [2]. All amyloid fibrils appear to be straight, unbranched fibers with a diameter of about 100 Å that stain with Congo Red, and exhibit red–green birefringence. The X-ray fiber diffraction patterns of all amyloid fibrils contain reflections that are characteristic of cross-β structure. In fact, a single model structure can fit the X-ray fiber diffraction patterns produced by amyloid fibrils derived from a diverse group of amyloid proteins [3]. This common structure of the amyloid protofiliament is composed of a number of β sheets twisting around a common helical axis, where the hydrogen bonding direction is parallel to the common helical axis [3].

The ability of a diverse group of proteins to fold into a common fibrillar structure has prompted the hypothesis that many, if not all, proteins can be induced to form amyloid fibrils [4]. Proteins and peptides that form amyloid can be separated into two classes based on the structure of their native non-amyloid state. In the first class are proteins that are folded, globular, and soluble; proteins that are unstructured or possess marginally stable structure under native conditions comprise the second class. The folded class of amyloidogenic proteins can be induced to form amyloid fibrils by subjecting them to mildly denaturing conditions where an aggregation-prone folding intermediate is populated. The proteins in this class include transthyretin, lysozyme, variable domain of immunoglobulin light chains and others [5,6]. Amyloid proteins and peptides that are unfolded or marginally folded under native conditions include the Alzheimer amyloid peptide (Aβ), islet amyloid polypeptide (IAPP), α-synuclein, and tau [6].

While it has been established that all amyloid fibrils possess a common core structure, it is not known whether the kinetic process of fibrillogenesis is also conserved. In this paper, we examine the fibrillogenesis of a peptide derived from residues 195–213 of the human prion protein, PrP (195–213). Many mutations that cause Gerstmann–Sträussler–Scheinker disease (GSS) and familial Creutzfeldt–Jakob disease (fCJD) are clustered in PrP (195–213). In addition, this peptide has been shown previously to form amyloid fibrils [7]. We have used a variety of biophysical techniques including fluorescence resonance energy transfer (FRET) methods that we have applied previously to study fibrillogenesis of Aβ [8]. We find that, unlike Aβ, fibrillogenesis of PrP (195–213) is an all-or-none process without appreciable population of small multimeric intermediates. Therefore, even though the core structures of all amyloid fibrils are highly similar, the fibrillogenesis pathways of individual amyloids are not conserved.

Correspondence to A. Chakrabartty, Ontario Cancer Institute, 610 University Ave., Toronto, Ontario M5G 2M9, Canada.
Fax: + 1 416 9466529, Tel.: + 1 416 9464501 (ext. 4910),
E-mail: chakrab@oci.utoronto.ca or N. R. Cashman, Centre for Research in Neurodegenerative Diseases, University of Toronto, Tanz Neuroscience Building, 6 Queen's Park Crescent West, Toronto, Ontario M5S 3H2, Canada. Fax: + 1 416 9781878,
Tel.: + 1 416 9781875, E-mail: neil.cashman@utoronto.ca

Abbreviations: PrP, prion protein; FRET, fluorescence resonance energy transfer; Aβ, Alzheimer amyloid peptide; IAPP, islet amyloid polypeptide; AEDANS, 5-((2-(*t*-BOC)-glutamylaminoethyl)amino) naphthalene-1-sulfonic acid; GSS, Gerstmann–Sträussler–Scheinker disease; fCJD, familial Creutzfeldt–Jakob disease

(Received 3 May 2001, revised 25 June 2001, accepted 20 July 2001)

MATERIALS AND METHODS

Peptide synthesis and fluorescent labeling of peptides

Peptide derivatives of PrP (195–213) (Fig. 1) were synthesized using solid phase chemistry on the Perseptive Biosystems 9050 peptide synthesizer. 9-Fluorenylmethoxy carbonyl (FMOC) was used as the α-amino protecting group for amino acids, and *O*-(7-azabenzotriazol-1-yl)-1,1,3,3,-tetramethyluronium hexafluorophosphate (HATU), PerSeptive Biosystems, GmbH, Hamburg, Germany, catalogue no. GENO76523, lot no. 217419, was used as activator of carboxylic group. The peptides were cleaved from the resin (PAL-PEG-PS, PerSeptive Biosystems, Warrington, UK,

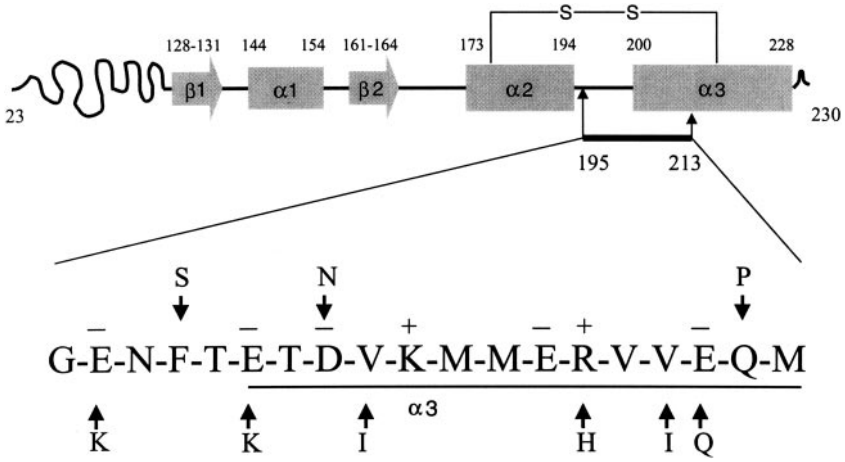

Fig. 1. The sequence of PrP (195–213) peptide. (Upper) Schematic representation of the NMR-derived secondary structure of human rPrP (23–230) [13]. (Lower) The sequence of PrP (195–213) peptide. Three mutations linked with GSS are listed above the PrP (195–213) sequence. Six mutations linked with fCJD are listed below the sequence of PrP (195–213). The charges of various residues are indicated above the peptide sequence. The fourteen residues of the third helix (α3) are underlined.

catalogue no.; Gen913383, lot no. 9812005) with a trifluoroacetic acid/anisole/triispropylsilane 90 : 8 : 2 (v/v) mixture. Synthesis products were precipitated with ice-cold ether, recovered by centrifigation, washed three times in ether, dissolved in 6.5 M guanidine/HCl, and purified by RP-HPLC on a C_{18} column. Peptide identity was confirmed by mass spectrometry.

Prior to fluorescent labeling, a glycine residue was added to the N-terminus of PrP (195–213) to act as a flexible linker between the fluorophore and peptide. Either a tryptophan residue or 5-((2-(*t*-BOC)-glutamylaminoethyl)amino) naphthalene-1-sulfonic acid (Molecular Probes) was then coupled to this extended PrP (195–213) sequence during peptide synthesis to create Trp-PrP (195–213) or AEDANS-PrP (195–213), respectively.

Purified peptides were lyophilized, and dissolved in 10% hexafluoroisopropanol (HFIP) and the peptide concentration was determined via tryptophan absorbance at 281 nm with an extinction coefficient [9] of 5690 $cm^{-1}\cdot M^{-1}$ or AEDANS absorbance at 338 nm with an extinction coefficient [10] of 6500 $cm^{-1}\cdot M^{-1}$. The stock solutions were stored at −20 °C until required.

Fluorescence spectroscopy

Fluorescence intensity was measured at room temperature using a Photon Technology International QM-1 fluorescence spectrophotometer equipped with excitation intensity correction. Emission spectra from 300 nm to 550 nm were collected (ex = 281 nm, 0.1–1 second·nm^{-1}, bandpass = 2 nm for excitation and emission). Cuvettes with 1-cm path lengths and volumes of either 0.5 mL or 3 mL were used. Samples were prepared at 1 : 1 ratio (w/w) of Trp-PrP (195–213) and AEDANS-PrP (195–213). To obtain the desired concentrations, appropriate amounts of peptide stock solutions in 10% HFIP were mixed, lyophilized, and dissolved in the appropriate buffer on the day of the experiment.

Turbidity measurement

To monitor aggregation, the UV absorbance at 400 nm of PrP (195–213) was measured with a Milton Roy Spectronic 300 Array UV spectrophotometer.

Circular dichroism

Far-UV circular dichroism spectra were recorded on an Aviv circular dichroism spectrometer model 62DS (Lakewood, NJ, USA) at 25 °C using quartz cells with a path length of 0.1 cm. Spectra were obtained from 195 nm to 260 nm, with a 1.0-nm step, 1.0-nm bandwidth, and 4-s collection time per step. The experimental data were expressed as mean residue ellipticity (θ) (deg·cm^2·$dmol^{-1}$).

Electron microscopy

Samples were placed on carbon-coated pioloform grid, blotted to remove excess sample and negatively stained with 1% (w/v) phosphotungstic acid, pH 7. The peptide assemblies were observed in a Hitachi 7000 operated with an accelerating voltage of 75 kV and images were recorded on film.

RESULTS

PrP (195–213) peptide displays minor helical propensity

The structure of recombinant prion proteins has been solved by NMR in three species: mouse 23–231 [11], hamster 29–231 [12], and human 23–230 [13]. As shown in Fig. 1, 14 residues in C-terminal region of the human PrP (195–213) peptide correspond to the third helix of the NMR structure of PrP [13]. Helical propensity of residues 195–213 could also be predicted (data not shown) from a modified form of Lifson–Roig helix-coil theory, and helix propagation parameters measured in alanine-based peptides [14,15]. Circular dichroism of PrP (195–213) in $NaCl/P_i$ (120 mM NaCl, 10 mM phosphate buffer) at pH 7.0 revealed that the peptide in solution was predominantly unstructured (displaying a strong negative CD band at 198 nm), but also possessed a small amount of helical structure (displaying a weak negative band around 222 nm). In the presence of the helix-promoting agent HFIP 10%, helical structure of the

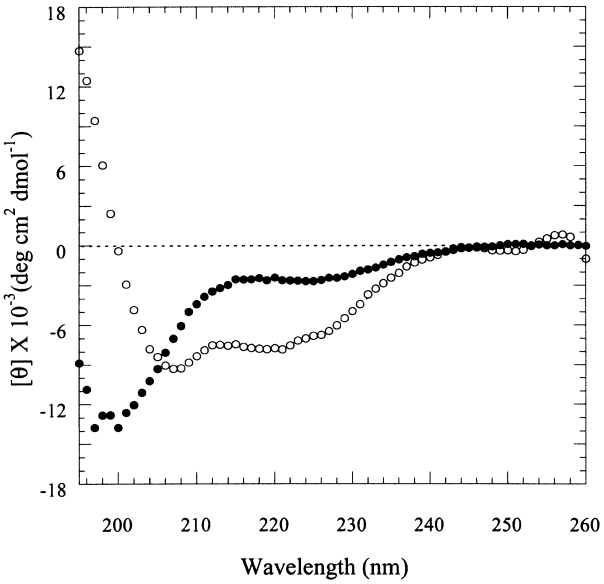

Fig. 2. Far-UV CD spectra of PrP (195–213) peptide in NaCl/P_i, pH 7 in the absence (●) and presence of 10% HFIP (○). PrP (195–213) in NaCl/P_i, pH 7.0 had a negative CD band at 198 nm and a weak negative band around 222 nm suggesting the presence of a small amount of α helix. In the presence of 10% HFIP, PrP (195–213) was predominantly α helical in structure with characteristic negative CD bands at 208 nm and 222 nm and a positive band at 192 nm.

peptide was more pronounced, as shown by characteristic minima at 208 nm and 222 nm (Fig. 2).

Self-association of PrP (195–213) monitored by FRET

We developed a sensitive method to monitor self-association of PrP (195–213) peptide monomers based on FRET. This technique has been applied by us [8] and others [16] to examine the aggregation of amyloid Aβ peptide [8]. In this method, donor and acceptor fluorophores are present on separate monomeric peptides and intermolecular energy transfer reports on the spatial proximity resulting from association or aggregation. Notably, FRET is sensitive to the association of peptide monomers in small soluble oligomers such as dimers and tetramers [8,16] that would not be detectable by other techniques, such as turbidity (see below).

In these experiments, aliquots of PrP (195–213) were labeled with the FRET donor tryptophan and other aliquots were labeled with the FRET acceptor AEDANS. Donor-labeled peptide, Trp-PrP (195–213) (0.125 mg·mL^{-1}), was mixed with acceptor-labeled peptide, AEDANS-PrP (195–213) (0.125 mg·mL^{-1}) at various pH values between 1.6 and 7.1. The fluorescence emission spectra of the peptide preparations were measured using an excitation wavelength of 281 nm, which causes significant excitation of Trp fluorophores but only slight excitation of AEDANS fluorophores. The emission spectra of the peptide samples at different pH indicated that lowering of pH from 7.1 to 1.6 was associated with two phenomena: quenching of Trp emission and increased sensitization of AEDANS emission (Fig. 3), thus demonstrating hallmarks of FRET. Therefore, it appears that low pH triggers the association of PrP (195–213) peptides into oligomers or aggregates at lower pH.

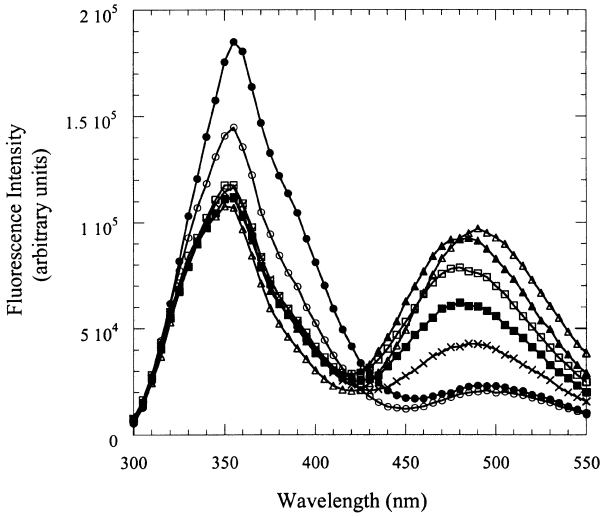

Fig. 3. Effect of pH on fluorescence emission spectra of mixtures of Trp- and AEDANS-PrP (195–213) peptides. Trp-PrP (195–213) (0.125 mg·mL^{-1}) was mixed with AEDANS-PrP (195–213) (0.125 mg·mL^{-1}) in 120 mM NaCl, 2 mM sodium phosphate, and 2 mM sodium citrate at various pH values between 1.6 and 7.1. The fluorescence emission spectra of the peptide preparations were measured using an excitation wavelength of 281 nm, pH 7.09 (●), pH 6.12 (○), pH 3.91 (×), pH 3.72 (■), 3.62 (□), 3.07 (▲), 1.63 (△).

The following procedure was used to obtain a quantitative measure of the degree of association. AEDANS intensities from 425 to 525 nm were integrated and this value was expressed as a ratio vs. the integrated intensities of Trp from 300 to 400 nm. The degree of association is directly proportional to this acceptor/donor ratio. The acceptor/donor ratios calculated from Fig. 3 were plotted as a function of pH and a sigmoidal titration curve was obtained (Fig. 4A). The midpoint of the pH titration occurred at pH 3.90, which is very close to the pK_a of the sidechains of Asp or Glu [17]. This suggests that neutralization of Asp and Glu sidechain carboxyl groups of PrP (195–213) can trigger self-association of the peptides.

Aggregation of PrP (195–213) is cooperative and small oligomers are not populated at equilibrium

As mentioned above, the FRET method for assessing the self-association tendency of PrP (195–213) is capable of detecting the formation of small oligomers as well as the formation of large aggregates. Measurement of turbidity is another method for assessing peptide aggregation [18]; however, this method will not detect the formation of small oligomers. FRET and turbidity measurements, used in tandem, can evaluate whether the aggregation process is all-or-none, or whether oligomeric intermediates are populated during the course of aggregation.

The pH-dependent changes in turbidity of PrP (195–213) were monitored over the range pH 1.6–7.1 and correlated with FRET measurements (Fig. 4A). The pH-titration curves obtained from both FRET and turbidity measurements were superimposable. This observation suggests that PrP (195–213) aggregates that form as the pH is lowered are predominantly large, and oppose the formation of small oligomers

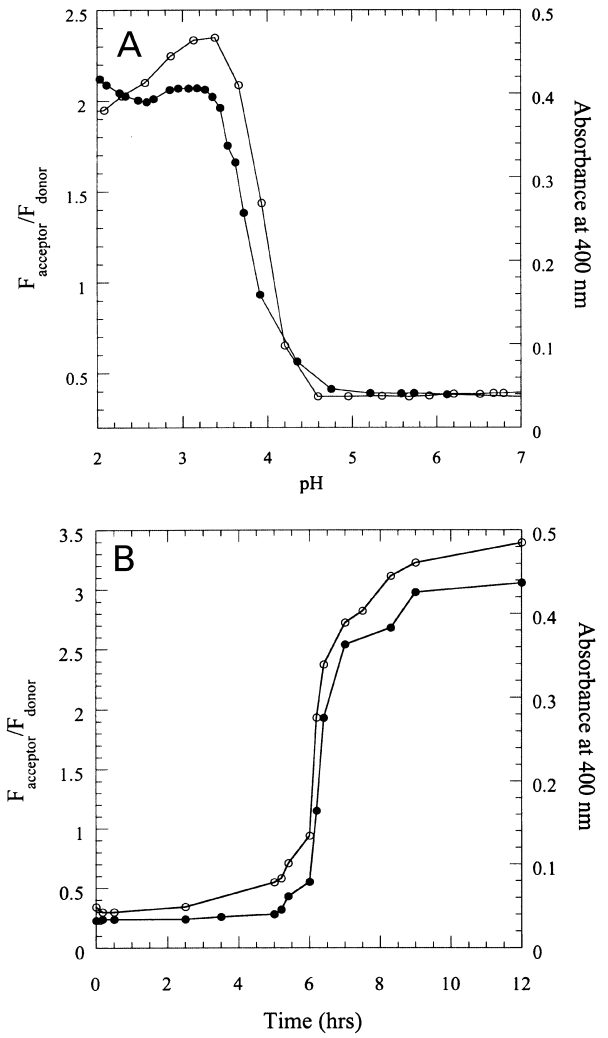

Fig. 4. pH- and time-dependence of peptide association/aggregation in mixtures of Trp- and AEDANS-PrP (195–213) peptide. (A) pH-dependence of association/aggregation of PrP (195–213) peptide. (B) Time-dependence of association/aggregation of PrP (195–213) peptide. Peptide association was determined by FRET analysis and expressed as the ratio of acceptor to donor fluorescence ($F_{acceptor}/F_{donor}$) (●). Peptide aggregation was detected by turbidity changes measured as absorbance at 400 nm (○).

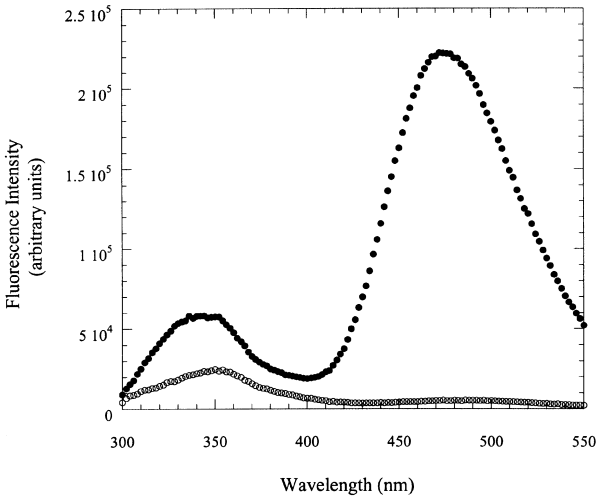

Fig. 5. FRET measurements of the aggregated mixtures of AEDANS- and Trp-PrP (195–213) before and after centrifugation. Fluorescence spectrum of the uncentrifuged aggregate suspension (●); Fluorescence spectrum of the centrifuged supernatant (○).

that would contribute to FRET but not to turbidity. Thus, the acid-induced aggregation of PrP (195–213) appears to be an all-or-none reaction in which oligomeric intermediates are not populated.

To investigate whether small oligomeric states of PrP (195–213) are populated transiently, the time course of aggregation/association at pH 2.0 was monitored using both FRET and turbidity measurements. The pH 2.0 point was chosen because both FRET and turbidity values were maximal and on the upper plateau region of the pH titration curves. The kinetic curves obtained from the FRET and turbidity measurements both possessed a lag time of 6 h and were superimposable at pH 2.0 (Fig. 4B). Furthermore, the correlation between FRET and turbidity measurements was highly statistically significant ($r = 0.988$, $P = 0.0001$). This indicates that any oligomeric intermediates that form prior to the formation of large aggregates are very short-lived and rapidly go on to form large aggregates, consistent with an all-or-none mechanism.

To confirm that soluble oligomeric forms of PrP (195–213) are not populated under equilibrium conditions, FRET measurements were taken on an aggregated sample of peptide before and after centrifugation at 16 000 ***g*** (Fig. 5). In the uncentrifuged aggregate suspension, a prominent FRET signal was observed, indicative of peptide–peptide association (see above). In the centrifuged supernatant, the acceptor/donor ratio was 0.215, identical to the ratio of unassociated peptides prior to aggregation (Fig. 4B). Thus, all of the soluble peptide in the aggregated sample appeared monomeric and not oligomeric.

It is possible to calculate the critical concentration for PrP (195–213) polymerization by determining the concentration of monomeric peptide in the centrifuged supernatant. Our estimate for this number is 18 μM. For the sake of comparison, the critical concentration for polymerization of the Alzheimer amyloid peptide (Aβ40) is estimated to be between 10 and 40 μM [18].

Formation of β structure accompanies aggregation of PrP (195–213) peptide

Changes in the secondary structure of PrP (195–213) during the time course of aggregation at pH 2.6 was assessed by CD spectroscopy. The CD spectrum of PrP (195–213) prior to aggregation possessed a minimum at 201 nm and a small shoulder at 220 nm (Fig. 6). This spectrum is indicative of a predominantly unstructured peptide that may also possess a small amount of α helical structure. After aggregation, the CD spectrum possessed a single minimum at 218 nm (Fig. 6), typical of β structure.

Aggregates from PrP (195–213) peptide are fibrillar

Freshly prepared mixtures of Trp- and AEDANS-PrP (195–213), which were shown to be nonaggregated by both FRET and turbidity measurements, were examined by negative

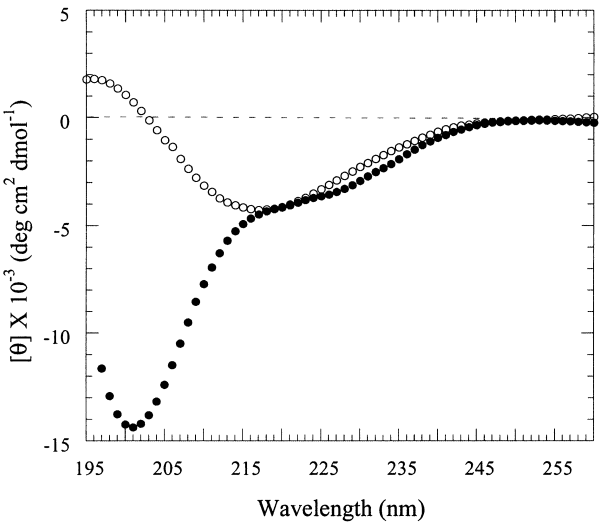

Fig. 6. Secondary structure of PrP (195–213) peptide before and after aggregation. CD spectra of Trp-PrP (195–213) (0.25 mg·mL^{-1}) in NaCl/P_i, pH 2.6 before (●) and after (○) aggregation.

stain electron microscopy. Electron micrographs of these preparations contained some insoluble material with flexible fibrous structure; however, their morphology was different from typical amyloid fibrils (Fig. 7A). On the other hand, preparations of Trp- and AEDANS-PrP (195–213) that were aggregated contained many long amyloid fibrils ≈ 100 Å in diameter and several μm in length; helical twisting and protofilament substructure was observed (Fig. 7B).

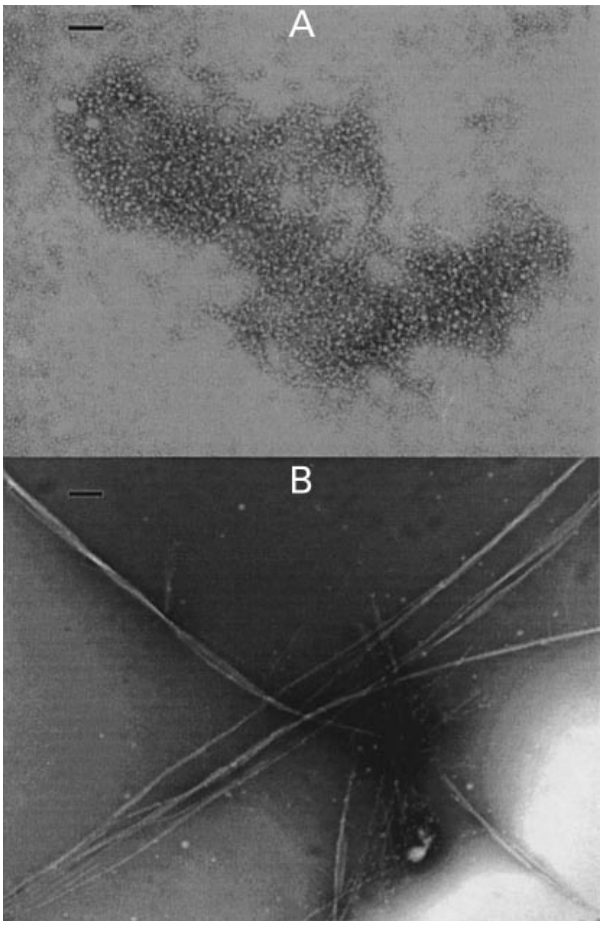

Fig. 7. Negative stain electron micrograph of aggregated mixtures of AEDANS- and Trp-PrP (195–213). Samples contained 0.125 mg·mL^{-1} each of Trp- and AEDANS-PrP (195–213) in 120 mM NaCl, 2 mM sodium phosphate and 2 mM sodium citrate, pH 2.0. (A) Electron micrograph of sample prior to aggregation. (B) Electron micrograph of sample after the occurrence of aggregation. Scale bars, 200 nm.

DISCUSSION

We have shown, using FRET and turbidity measurements in tandem, that PrP (195–213) aggregation is a highly cooperative process that apparently occurs by an all-or-none mechanism, without appreciable population of small multimeric intermediates. As the operational distance limitation of FRET is approximately 40 Å, this method could be conceivably applied to larger PrP fragments, e.g. PrP (90–231), or even to intact PrP.

The pH dependence of aggregate-fibril formation has an apparent pK_a of 3.9, suggesting that the assembly process is promoted by protonation of the sidechain carboxyl groups of Asp and Glu residues in PrP (195–213). The effect of pH on PrP and PrP fragments has been well studied. It is thought that PrP conversion *in vivo* occurs in the acidic environment of the endosomal–lysosomal system [19–22]. Recombinant forms of human PrP (90–231) [23], human PrP (91–231) [24], and mouse PrP (121–231) [25] form an equilibrium folding intermediate at low pH in the presence of either 1 M guanidine hydrochloride or 3.5 M urea. The equilibrium intermediate of human PrP (91–231) with disulfide bonds intact has a tendency to aggregate [24]. The pH-induced conversion of human PrP (90–231) and mouse PrP (121–231) from the native state to the equilibrium folding intermediate occur with an apparent pK_a of 5.1 [23] and 4.5 [25], respectively. These apparent pK_a values suggest the involvement of either acidic residues (i.e. Asp and Glu) or histidines. Electrostatic calculations, based on the solution structures of mouse PrP (121–231) and Syrian hamster PrP (90–231), have suggested that protonation of the following acidic residues, which are listed in rank order, causes the greatest destabilization of the native state of PrP and may facilitate the formation of the equilibrium folding intermediate: E196, D178, D202, E152, D144, D147, E146, and E211 [26]. Calculations also implicate the involvement of H96 and H111 in aggregation of PrP [26]. In the present study, PrP (195–213) also possess the property of forming β structure and amyloid fibrils at lower pH. PrP (195–213) contains E196, E200, D202, E207, and E211, which includes three of the acidic amino acids listed above as most important in the pH transition of recombinant PrP^C to a β sheet form.

What is the mechanism by which protonation of acidic residues promotes aggregation-fibrillogenesis in PrP (195–213)? Two scenarios might apply. First, peptide aggregation may be promoted by isoelectric precipitation that occurs when the pH is lowered to the peptide's isoelectric point where net charge is zero. Second, aggregation may be prevented by the repulsion of acidic sidechains at higher pH,

and neutralization of these sidechains at lower pH could therefore promote fibrillogenesis. PrP (195–213) peptide contains four Glu, one Asp, one Lys, one Arg, and a free α amino group at the N-terminus (the C-terminus is amidated). Based on the typical pK_a values of the ionizable groups present, the isoelectric point of the peptide would probably be between 3 and 4. At pH2 the peptide would have a net charge of +3. As fibrils form readily at pH2 (Fig. 7), this reduces the likelihood of isoelectric precipitation being the cause of pH-dependent aggregation (Figs 4A and 7). Thus, the second scenario, that fibrillogenesis at higher pH is prevented by repulsion of acidic sidechains, provides a more plausible explanation for our findings. This explanation implies that the repulsion of acidic sidechains (above pH 4) is more disruptive to aggregation-fibrillogenesis than the repulsion of basic sidechains (below pH 4). Perhaps there is a larger intermolecular separation distance between positive charges in the three-dimensional structure of the fibril compared to the separation distance between the negative charges.

The process of fibril formation by PrP (195–213) exhibited a well-defined lag phase (Fig. 4B). Two non-exclusive models have been proposed for the conversion of PrP^C to PrP^{Sc}: seeded polymerization and template-assistance. A lag phase is a prominent feature of both proposed mechanisms. In the seeded polymerization model, PrP^{Sc} is considered to be an aggregate and the aggregation process is believed to induce a transformation of PrP^C to the β-structured amyloid polymer. Oligomerization of a number of PrP molecules represents the formation of a nucleus or seed and is proposed to be a slow process that accounts for the lag phase [27–29]. The template-assistance model proposes that the lag phase is caused by the presence of a large kinetic barrier to the conversion of monomeric PrP^C to monomeric PrP^{Sc}. In this model, a single PrP^{Sc} molecule is proposed to act as a template that reduces the kinetic barrier and catalyzes conversion of monomeric PrP^C to PrP^{Sc} [30,31]. From the results of this study, we conjecture that the lag phase observed with fibrillogenesis of PrP (195–213) is a result of the slow formation of an oligomeric nucleus for the following reasons. Unlike PrP^C, monomeric PrP (195–213) contains at most a very small amount of helical structure with marginal stability. Folding and unfolding of small peptides containing single helices occurs relatively rapidly [32–34]; consequently, conversion of PrP (195–213) from its partially helical state to a monomeric state, where the peptide possesses dihedral angles in the β sheet region of the Ramachandran plot, is also expected to occur rapidly. Furthermore, because of the small size of the PrP (195–213) peptide, it is unlikely that the molecule can form a monomeric H-bonded β sheet structure that would be equivalent to a monomeric PrP^{Sc} molecule. Finally, our finding that aggregation-fibrillogenesis of this peptide follows an all-or-none process indicates that small oligomers are unstable. From this evidence, we surmise that the observed lag phase reflects the slow formation of oligomeric nuclei. Once formed, the nuclei rapidly grow into amyloid fibrils.

The all-or-none fibrillogenesis mechanism of PrP (195–213) differs markedly from the kinetic mechanism of other amyloid. Fibrillogenesis of the Alzheimer Aβ peptide appears to proceed through a number of oligomeric intermediates that are transiently populated for time periods ranging from minutes to hours. Prior to fibril formation, Aβ associates into small oligomers ranging from dimers to tetramers [8,16]. Other intermediates of Aβ fibrillogenesis include soluble spherical aggregates [8,35–37] and protofibrils [37,38]. Transient formation of spherical aggregates has also been observed during fibrillogenesis of α-synuclein [39] and IAPP [40]. This variation in whether intermediate states are stably populated during fibrillogenesis demonstrates that different amyloid proteins utilize different pathways to arrive at the same core structure.

ACKNOWLEDGEMENTS

This work was supported by a grant to A. C. from the Canadian Institutes for Health Research (CIHR), by a grant to N. R. C. from Caprion Pharmaceuticals (Montreal, Quebec, Canada), and by a grant to P. E. F. from CIHR, Ontario Mental Health and the Alzheimer's Society of Ontario.

REFERENCES

1. Sipe, J.D. & Cohen, A.S. (2000) Review: history of the amyloid fibril. *J. Struct. Biol.* **130**, 88–98.
2. Serpell, L.C., Sunde, M. & Blake, C.F. (1997) The molecular basis of amyloidosis. *Cell Mol. Life Sci.* **53**, 871–887.
3. Sunde, M., Serpell, L.C., Bartlam, M., Fraser, P.E., Pepys, M. & Blake, C.F. (1997) Common core structure of amyloid fibrils by synchrotron X-ray diffraction. *J. Mol. Biol.* **273**, 729–739.
4. Chiti, F., Webster, P., Taddei, N., Clark, A., Stefani, M., Ramponi, G. & Dobson, C.M. (1999) Designing conditions for *in vitro* formation of amyloidprotofilaments and fibrils. *Proc. Natl Acad. Sci. USA* **96**, 3590–3594.
5. Dobson, C.M. (1999) Protein misfolding, evolution and disease. *Trends Biochem. Sci.* **24**, 329–332.
6. Rochet, J.C. & Lansbury, P.T. (2000) Amyloid fibrillogenesis: themes and variations. *Curr. Opin. Struct. Biol.* **10**, 60–68.
7. Goldfarb, L.G., Brown, P., Haltia, M., Ghiso, J., Frangione, B. & Gajdusek, D.C. (1993) Synthetic peptides corresponding to different mutated regions of the amyloid gene in familial Creutzfeldt–Jakob disease show enhanced *in vitro* formation of morphologically different amyloid fibrils. *Proc. Natl Acad. Sci. USA* **90**, 4451–4454.
8. Huang, T.H.J., Fraser, P.E. & Chakrabartty, A. (1997) Fibrillogenesis of Alzheimer A beta peptides studied by fluorescence energy transfer. *J. Mol. Biol.* **269**, 214–224.
9. Edelhoch, H. (1967) Spectroscopic determination of tryptophan and tyrosine in proteins. *Biochemistry* **6**, 1948–1954.
10. Hudson, E.N. & Weber, G. (1973) Synthesis and characterization of two fluorescentsulfhydryl reagents. *Biochemistry* **12**, 4154–4161.
11. Riek, R., Hornemann, S., Wider, G., Glockshuber, R. & Wüthrich, K. (1997) NMR characterization of the full-length recombinant murine prion protein, mPrP (23231). *FEBS Lett.* **413**, 282–288.
12. Donne, D.G., Viles, J.H., Groth, D., Mehlhorn, I., James, T.L., Cohen, F.E., Prusiner, S.B., Wright, P.E. & Dyson, H.J. (1997) Structure of the recombinant full-length hamster prion protein PrP (29–231): the N terminus is highly flexible. *Proc. Natl Acad. Sci. USA* **94**, 13452–13457.
13. Zahn, R., Lin, A., Lührs, T., Riek, R., Schroetter, C., Garcia, F.L., Billeter, M., Calzolai, L., Wider, G. & Wüthrich, K. (2000) NMR solution structure of the human prion protein. *Proc. Natl Acad. Sci. USA* **97**, 145–150.
14. Doig, A.J., Chakrabatty, A., Klingler, T.M. & Baldwin, R.L. (1994) Determination of free energies of N-capping in alpha-helices by modification of the Lifson–Roig helix-coil therapy to include N- and C-capping. *Biochemistry* **33**, 3396–3403.
15. Rohl, C.A., Chakrabartty, A. & Baldwin, R.L. (1996) Helix propagation and N-cap propensities of the amino acids measured in

alanine-based peptides in 40 volume percent trifluoroethanol. *Protein Sci.* **5**, 2623–2637.
16. Garzon-Rodreguez, W., Sepulveda-Becerra, M., Milton, S. & Glabe, C.G. (1997) Soluble amyloid A beta (1–40) exists as a stable dimer at low concentrations. *J. Biol. Chem.* **272**, 21037–21044.
17. Rodwell, V.W. (1988) Structures and functions of proteins and enzymes: amino acids. In *Harper's Biochemistry* (Murray, R.K., Granner, D.K., Mayes, P.A. & Rodwell, V.W., eds), pp. 14. Appleton & Lange, Norwalk, Connecticut/San Mateo, CA.
18. Harper, J.D. & Lansbury, P.T. (1997) Models of amyloid seeding in Alzheimer's disease and scrapie: mechanistic truths and physiological consequences of the time-dependent solubility of amyloid proteins. *Annu. Rev. Biochem.* **66**, 385–407.
19. Arnold, J.E., Tipler, C., Laszlo, L., Hope, J., Landon, M. & Mayer, R.J. (1995) The abnormal isoform of the prion protein accumulates in late-endosome-like organelles in scrapie-infected mouse brain. *J. Pathol.* **176**, 403–411.
20. Mayer, R.J., Tipler, C., Laszlo, L., Arnold, J., Lowe, J. & Landon, M. (1994) Endosome-lysosomes and neurodegeneration. *Biomed. Pharmacother.* **48**, 282–286.
21. Taraboulos, A., Raeber, A., Borchelt, D.R., Serban, D. & Prusiner, S.B. (1992) Synthesis and trafficking of prion proteins in cultured cells. *Mol. Biol. Cell* **3**, 851–863.
22. Laszlo, L., Lowe, J., Self, T., Kenward, N., Landon, M., McBride, T., Farquhar, C., McConnell, I., Brown, J., Hope, J. & Mayer, R.J. (1992) Lysosomes as key organelles in the pathogenesis of prion encephalopathies. *J. Pathol.* **166**, 333–341.
23. Swietnicki, W., Petersen, R., Gambetti, P. & Surewicz, W. (1997) pH-dependent stability and conformation of the recombinant human prion protein PrP (90–231). *J. Biol. Chem.* **272**, 27517–27520.
24. Jackson, G.S., Hill, A.F., Joseph, C., Hosszu, L., Power, A., Waltho, J.P., Clarke, A.R. & Collinge, J. (1999) Multiple folding pathways for heterologously expressed human prion protein. *Biochem. Biophys. Acta* **1431**, 1–13.
25. Hornemann, S. & Glockshuber, R. (1998) A scrapie-like unfolding intermediate ofthe prion protein domain PrP (121–231) induced by acidic pH. *Proc. Natl Acad. Sci. USA* **95**, 6010–6014.
26. Warwicker, J. (1999) Modelling charge interactions in the prion protein: predictions for pathogenesis. *FEBS Lett.* **450**, 144–148.
27. Come, J.H., Fraser, P.E. & Lansbury, P.T. Jr (1993) A kinetic model for amyloid formation in the prion diseases: importance of seeding. *Proc. Natl Acad. Sci. USA* **90**, 5959–5963.
28. Jarrett, J.T. & Lansbury, P.T. Jr (1993) Seeding 'one-dimensional crystallization' of amyloid: a pathogenic mechanism in Alzheimer's disease and scrapie? *Cell* **73**, 1055–1058.
29. Lansbury, P.T. Jr & Caugher, B. (1995) The chemistry of scrapie infection: implications of the 'ice 9' metaphor. *Chem. Biol.* **2**, 1–5.
30. Prusiner, S.B. (1991) Molecular biology of prion diseases. *Science* **252**, 1515–1522.
31. Cohen, F.E., Pan, K.-M., Huang, Z., Baldwin, M.A., Fletterick, R.J. & Prusiner, S.B. (1994) Structural clues to prion replication. *Science* **264**, 530–531.
32. Cummings, A.L. & Eyring, E.M. (1975) Helix-coil transition kinetics in aqueous poly (α, L-glutamic acid). *Biopolymers* **14**, 2107–2114.
33. Williams, S., Causgrove, T.P., Gilmanshin, R., Fang, K.S., Callender, R.H., Woodruff, W.H. & Dyer, R.B. (1996) Fast events in protein folding: helix melting and formation in a small peptide. *Biochemistry* **35**, 691–697.
34. Clarke, D.T., Doig, A.J., Stapley, B.J. & Jones, G.R. (1999) The alpha-helix folds on the millisecond time scale. *Proc. Natl Acad. Sci. USA* **96**, 7232–7237.
35. Snyder, S., Ladror, U.S., Wade, W.S., Wang, G.T., Barret, L.W., Matayoshi, E.D., Huffaker, H.J., Krafft, G.A. & Holzman, T.F. (1994) Amyloid-beta aggregation: selective inhibition of aggregation in mixtures with different chain lengths. *Biophys. J.* **67**, 1216–1228.
36. Kowalewski, T.Z. & Holtzman, D.M. (1999) In situ atomic force microscopy studyof Alzheimer's beta-amyloid peptide on different substrates: new insights into mechanism of beta-sheet formation. *Proc. Natl Acad. Sci. USA* **96**, 3688–3693.
37. Harper, J.D., Wong, S.S., Lieber, C.M. & Lansbury, P.T. (1999) Assembly of Abeta amyloid protofibrils: an *in vitro* model for a possible early event in Alzheimer's disease. *Biochemistry* **38**, 8972–8980.
38. Walsh, D.M., Hartley, D.M., Kusumoto, Y., Fezoui, Y., Condron, M.M., Lomakin, A., Benedek, G.B., Selkoe, D.J. & Teplow, D.B. (1999) Amyloid beta-protein fibrillogenesis. Structure and biological activity of protofibrillar intermediates. *J. Biol. Chem.* **274**, 25945–25952.
39. Conway, K.A., Lee, S.J., Rochet, J.C., Ding, T.T., Williamson, R.E. & Lansbury, P.T. (2000) Acceleration of oligomerization, not fibrillization, is a shared property of both alpha-synuclein mutations linked to early-onset Parkinson's disease: implications for pathogenesis and therapy. *Proc. Natl Acad. Sci. USA* **97**, 571–576.
40. Goldsbury, C., Kistler, J., Aebi, U., Arvinte, T. & Cooper, G.J. (1999) Watching amyloid fibrils grow by time-lapse atomic force microscopy. *J. Mol. Biol.* **285**, 33–39.